## $9^{th}$ Workshop on Radiation Monitoring

## for the International Space Station

# Evaluation of Neutron Radiation Environment inside the International Space Station based on the Bonner Ball Neutron Detector Experiment

**H. Koshiishi, H. Matsumoto, A. Chishiki,**

**T. Goka, and T. Omodaka**

**Japan Aerospace Exploration Agency**

# 1. Introduction

Neutron radiation inside spacecrafts, major part of which is secondary produced by the interaction between high-energy cosmic-ray particle and spacecraft materials, has been remarked as one of the major contributors to astronaut dose.

# 1. Introduction

Neutron radiation inside spacecrafts, major part of which is secondary produced by the interaction between high-energy cosmic-ray particle and spacecraft materials, has been remarked as one of the major contributors to astronaut dose.

A Bonner Ball Neutron Detector (BBND) experiment was conducted for about 8 months in 2001 on the US Laboratory Module of the International Space Station (ISS), as part of the science program of NASA's Human Research Facility (HRF), in order to evaluate the neutron radiation environment inside the ISS.

# 1. Introduction

Neutron radiation inside spacecrafts, major part of which is secondary produced by the interaction between high-energy cosmic-ray particle and spacecraft materials, has been remarked as one of the major contributors to astronaut dose.

A Bonner Ball Neutron Detector (BBND) experiment was conducted for about 8 months in 2001 on the US Laboratory Module of the International Space Station (ISS), as part of the science program of NASA's Human Research Facility (HRF), in order to evaluate the neutron radiation environment inside the ISS.

In this presentation, results from the BBND experiment is reported.

# 2. Bonner Ball Neutron Detector

The BBND sensor consists of six $^3$He proportional counters covered with polyethylene moderators of various thickness and gadolinium eliminators.


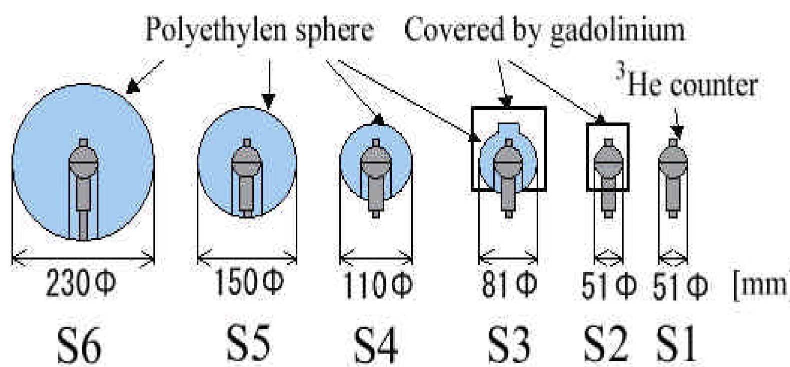

# 2. Bonner Ball Neutron Detector

The BBND sensor consists of six $^3$He proportional counters covered with polyethylene moderators of various thickness and gadolinium eliminators.

Each counter has different energy response function for incident neutron, which is obtained by irradiation experiments with numerical calculations.

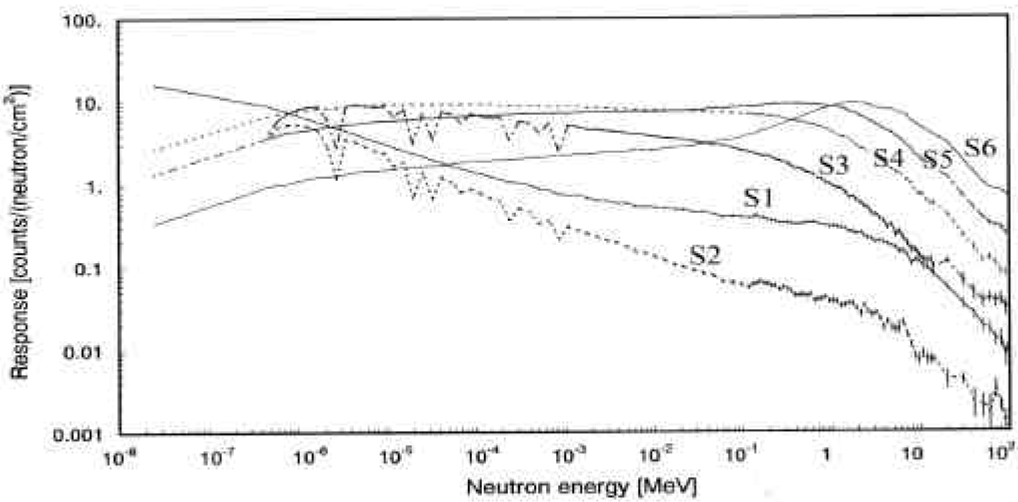

# 3. Measurements

Energy Range : Thermal (0.025eV) – 15MeV

Measurement Period :

23rd Mar. through 15th Nov. 2001 for about 8 months

corresponding to solar-activity maximum period

Altitude variation : 369km – 415km Average 394km

# 3. Measurements

Energy Range : Thermal (0.025eV) – 15MeV

Measurement Period :

23rd Mar. through 15th Nov. 2001 for about 8 months

corresponding to solar-activity maximum period

Altitude variation : 369km – 415km Average 394km

The BBND instruments was once relocated on 9th Aug. during the experimental period.

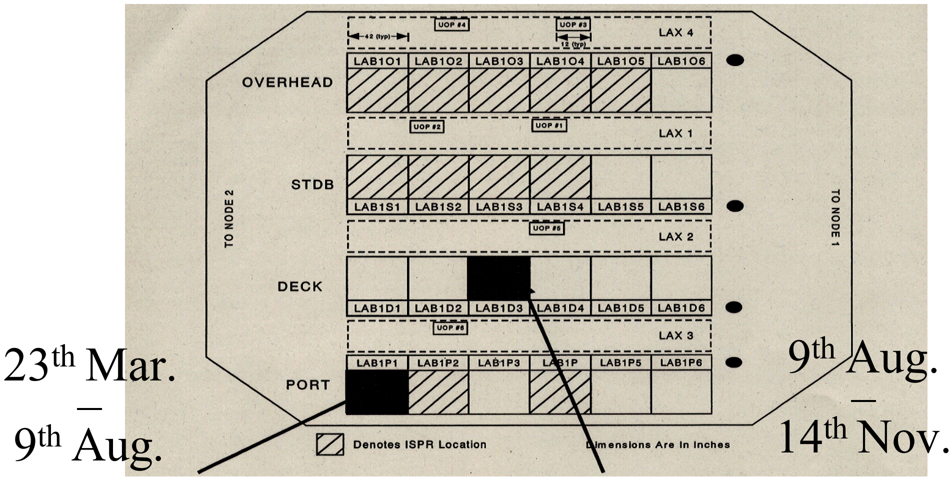

# 3. Measurements

Energy Range : Thermal (0.025eV) – 15MeV

Measurement Period :

23rd Mar. through 15th Nov. 2001 for about 8 months

corresponding to solar-activity maximum period

Altitude variation : 369km – 415km Average 394km

The BBND instruments was once relocated on 9th Aug. as during the experimental period. → Evaluation of neutron radiation environment under different shield conditions

# 4. Analyses

Differential Energy Spectrum

Thermal (0.025eV) – 15MeV 22bin

Unfolding method

Armstrong′ s albedo neutron data as an initial guess

1-minute

temporal resolution

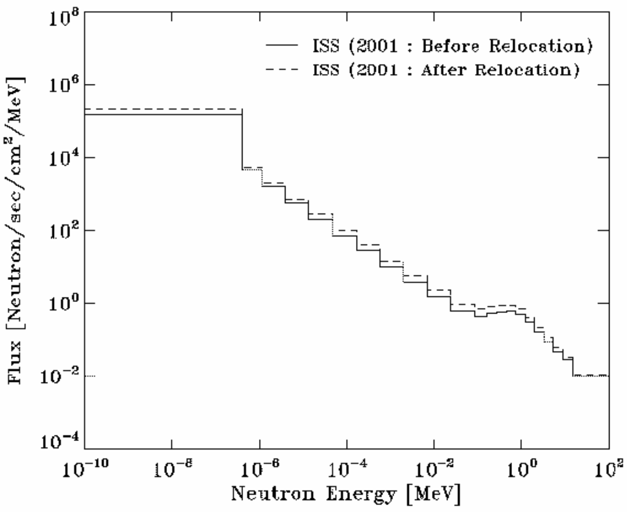

# 4. Analyses

Differential Energy Spectrum

Thermal (0.025eV) – 15MeV 22bin

Unfolding method

Armstrong′ s albedo neutron data as an initial guess

1-minute

temporal resolution

Dose-Equivalent

ICRP-74

conversion coefficient

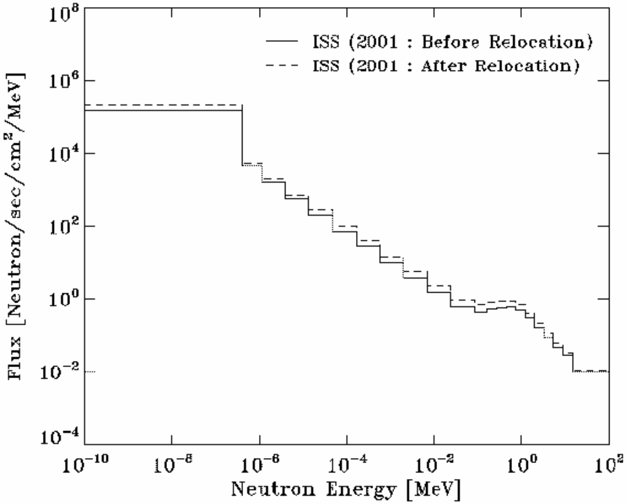

# 5. Dose-Equivalent Rate Variation

Average dose-equivalent rate 85µSv/d (before relocation)

109µSv/d (after relocation)

? 30% increase due to relocation even between the regulated racks for experimental instruments

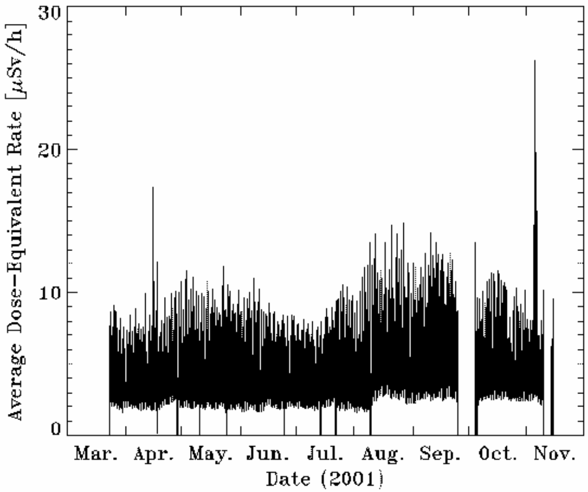

# 5. Dose-Equivalent Rate Variation

The lower boundary of dose-equivalent rate variation

? on orbits which do not pass through SAA region

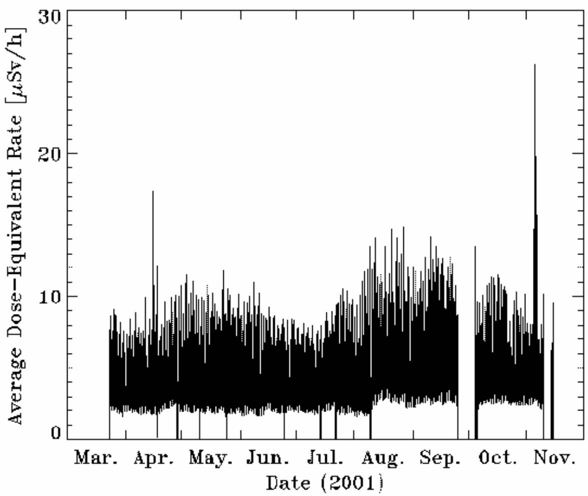

# 5. Dose-Equivalent Rate Variation

The lower boundary of dose-equivalent rate variation

? on orbits which do not pass through SAA region

The envelope of upper boundary

? due to altitude variation in SAA region

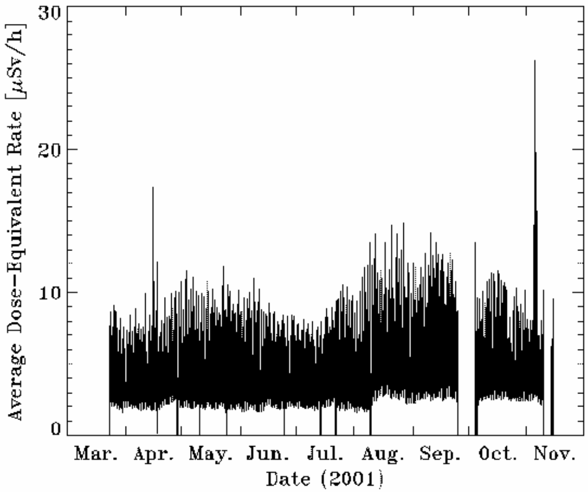


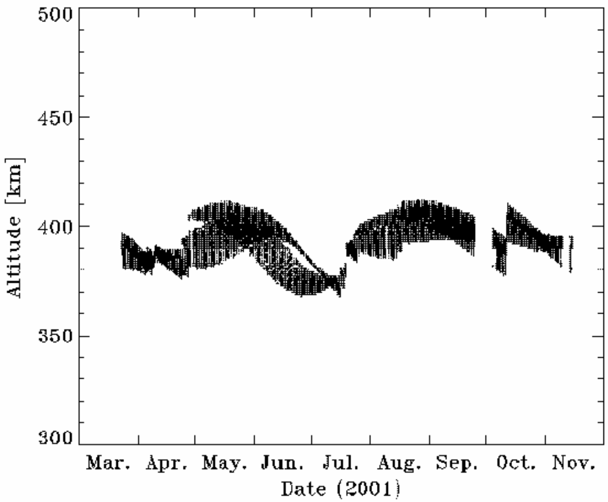

# 5. Dose-Equivalent Rate Variation

The lower boundary of dose-equivalent rate variation

? on orbits which do not pass through SAA region

The envelope of upper boundary

? due to altitude variation in SAA region

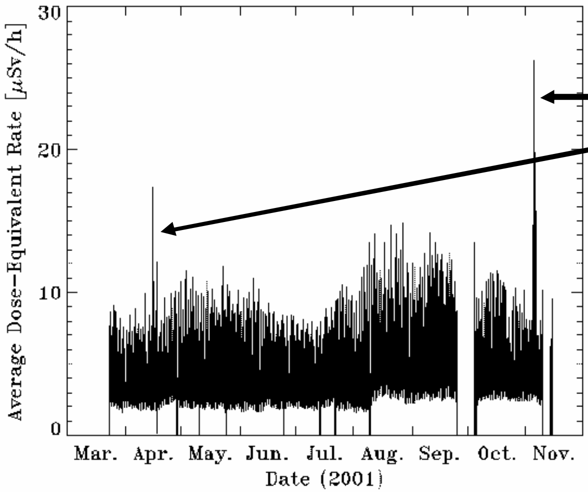


These spikes in April and November were caused by large solar flares associated with proton event.

# 6. Geographic Dose-Equivalent Rate Distribution

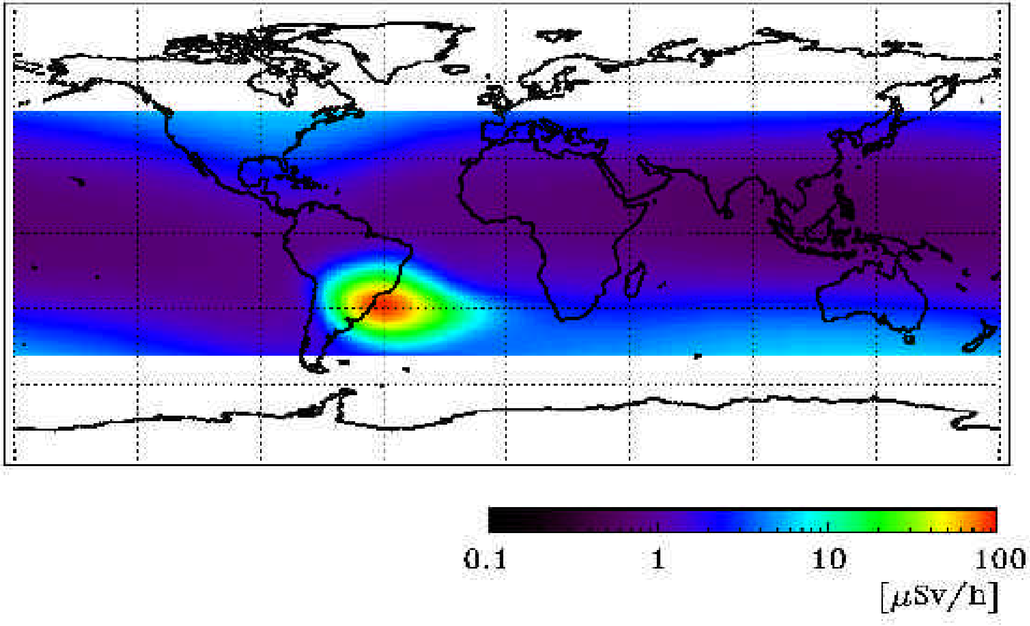

# 6. Geographic Dose-Equivalent Rate Distribution

The whole aspect of dose-equivalent rate distribution is due to geomagnetic cut-off rigidity distribution except in SAA region.

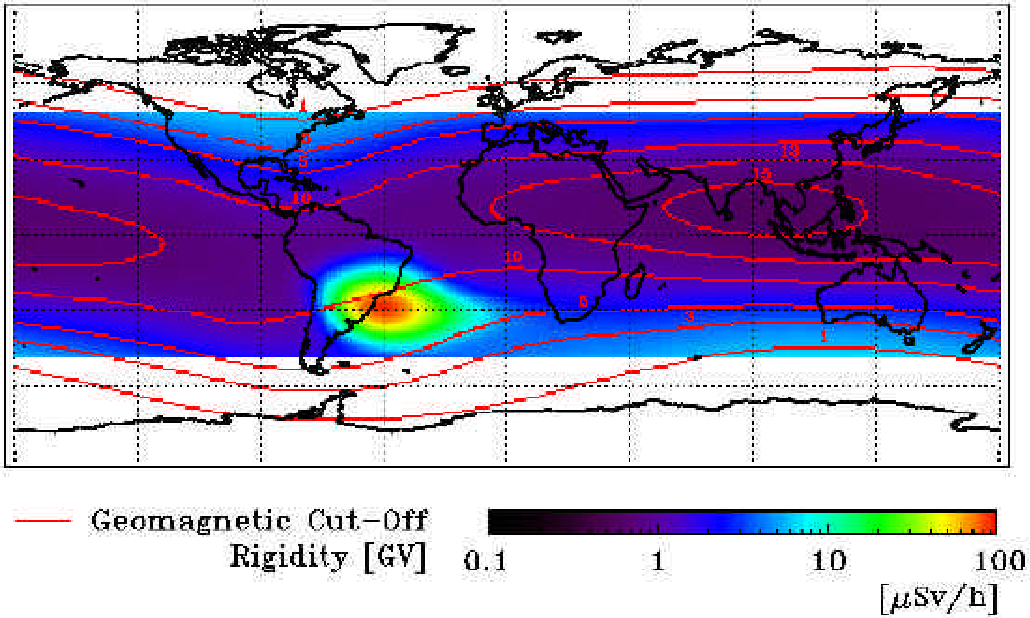

# 6. Geographic Dose-Equivalent Rate Distribution

The whole aspect of dose-equivalent rate distribution is due to geomagnetic cut-off rigidity distribution except in SAA region.

? GCR contribution and trapped-proton contribution to dose-equivalent rate can be handled separately.

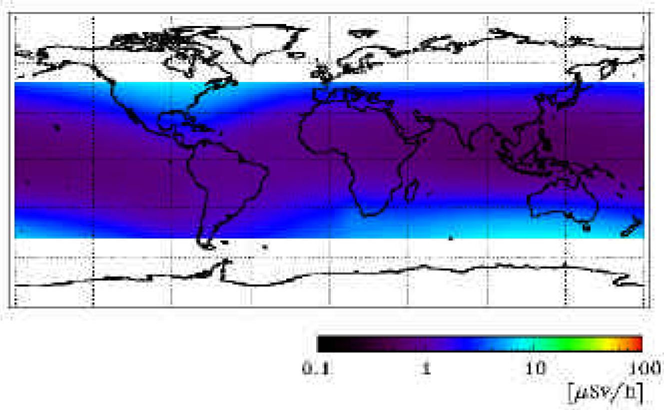


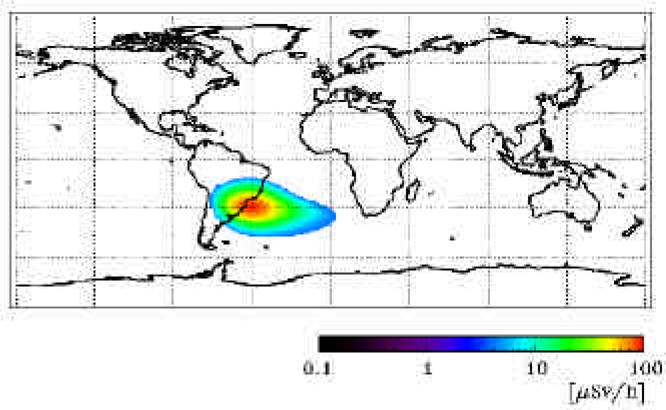

# 7. Geomagnetic Cut-Off Rigidity and Trapped-Proton Integrated Flux

GCR contributed dose-equivalent rate as a function of geomagnetic cut-off rigidity

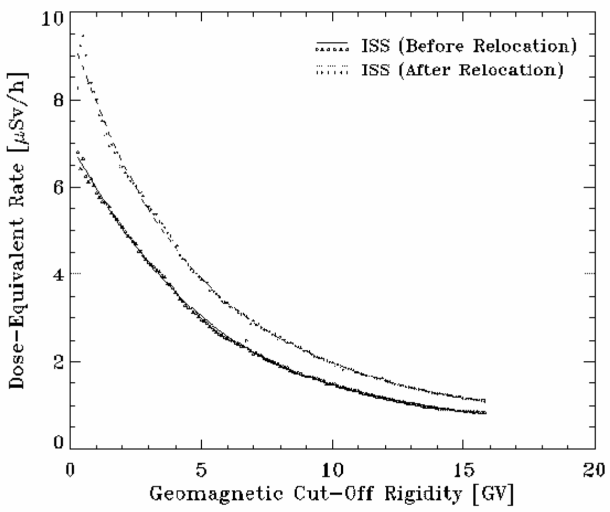

# 7. Geomagnetic Cut-Off Rigidity and Trapped-Proton Integrated Flux

GCR contributed dose-equivalent rate as a function of geomagnetic cut-off rigidity

Trapped-proton contributed dose-equivalent rate as a function of trapped-proton integrated flux (10-400MeV)

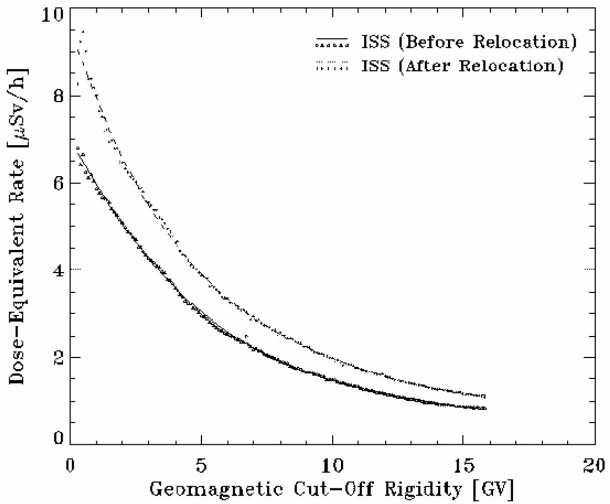


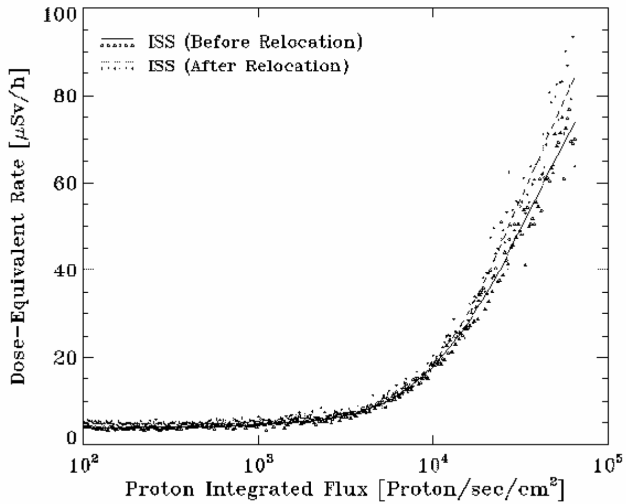

# 8. Altitude Dependence of Dose-Equivalent Rate

Two relations to describe dose-equivalent rate distribution

+

Geomagnetic cut-off rigidity distribution calculated by CREAM86 code

+

Trapped-proton integrated flux distribution (10-400MeV) calculated by AP-8 MAX code

?

Altitude dependence of dose-equivalent rate is briefly estimated.

# 8. Altitude Dependence of Dose-Equivalent Rate

Geomagnetic cut-off rigidity and trapped-proton integrated flux are calculated from altitude of 300km through 500km in each 10km step. Each dose-equivalent rate distribution is estimated separately, and summed at final.

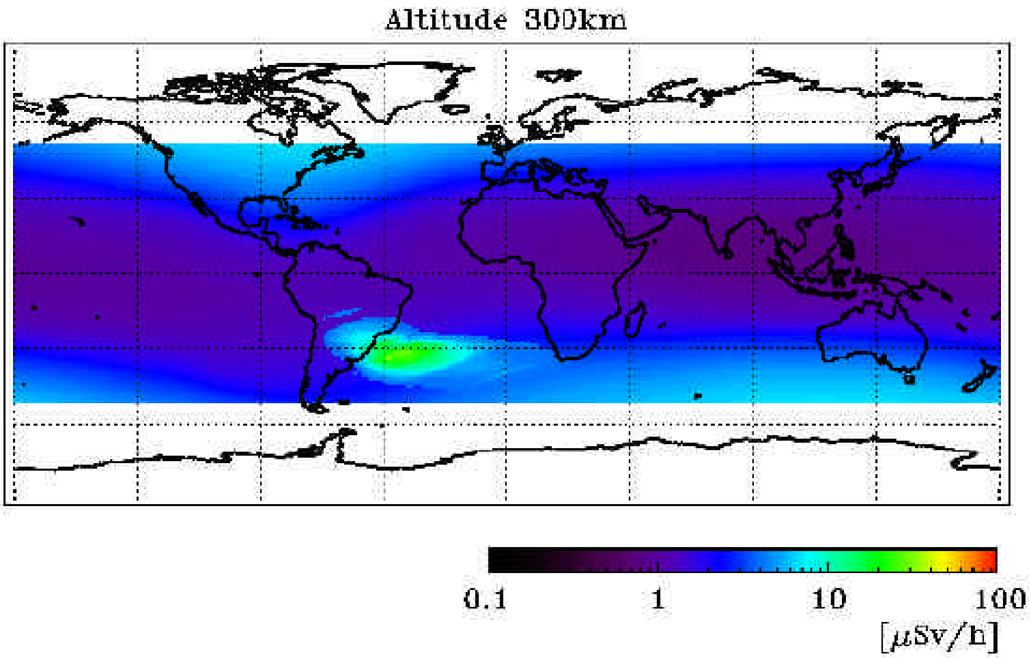

# 8. Altitude Dependence of Dose-Equivalent Rate

Geomagnetic cut-off rigidity and trapped-proton integrated flux are calculated from altitude of 300km through 500km in each 10km step. Each dose-equivalent rate distribution is estimated separately, and summed at final.

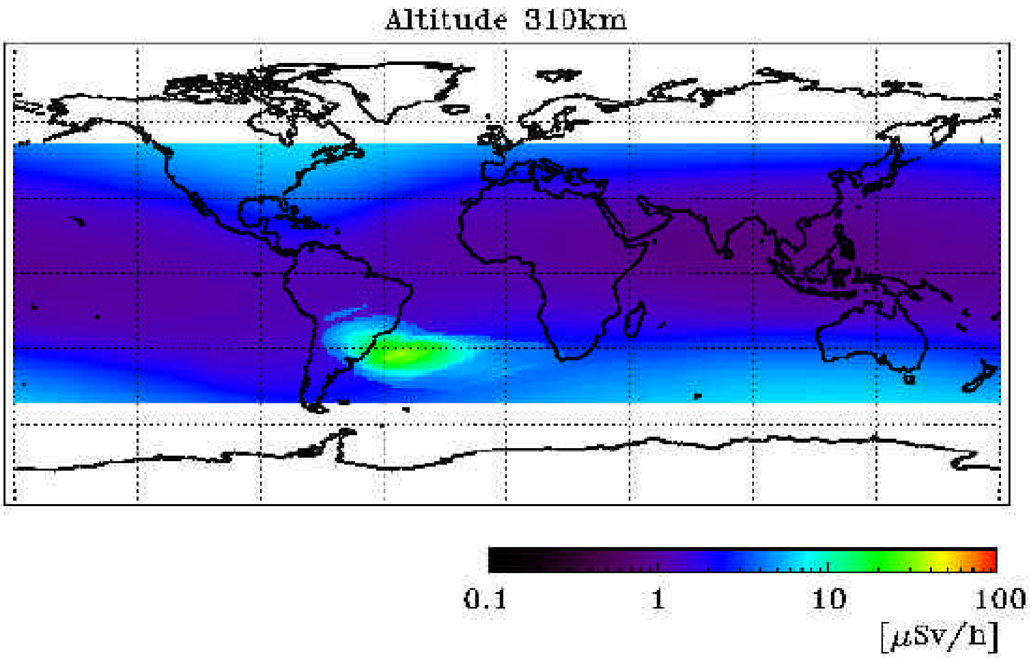

# 8. Altitude Dependence of Dose-Equivalent Rate

Geomagnetic cut-off rigidity and trapped-proton integrated flux are calculated from altitude of 300km through 500km in each 10km step. Each dose-equivalent rate distribution is estimated separately, and summed at final.

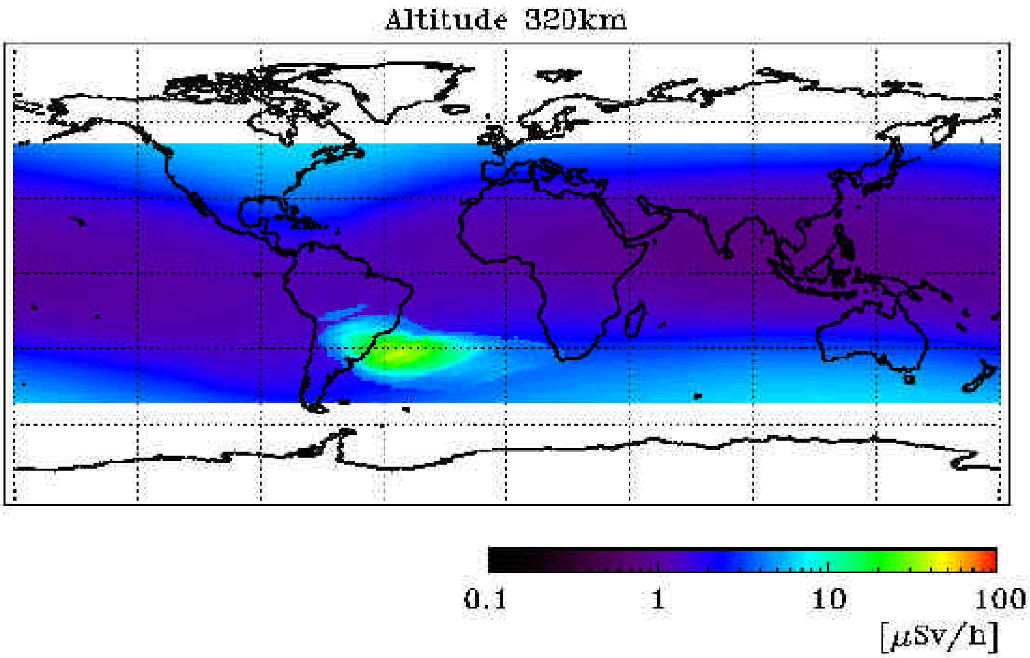

# 8. Altitude Dependence of Dose-Equivalent Rate

Geomagnetic cut-off rigidity and trapped-proton integrated flux are calculated from altitude of 300km through 500km in each 10km step. Each dose-equivalent rate distribution is estimated separately, and summed at final.

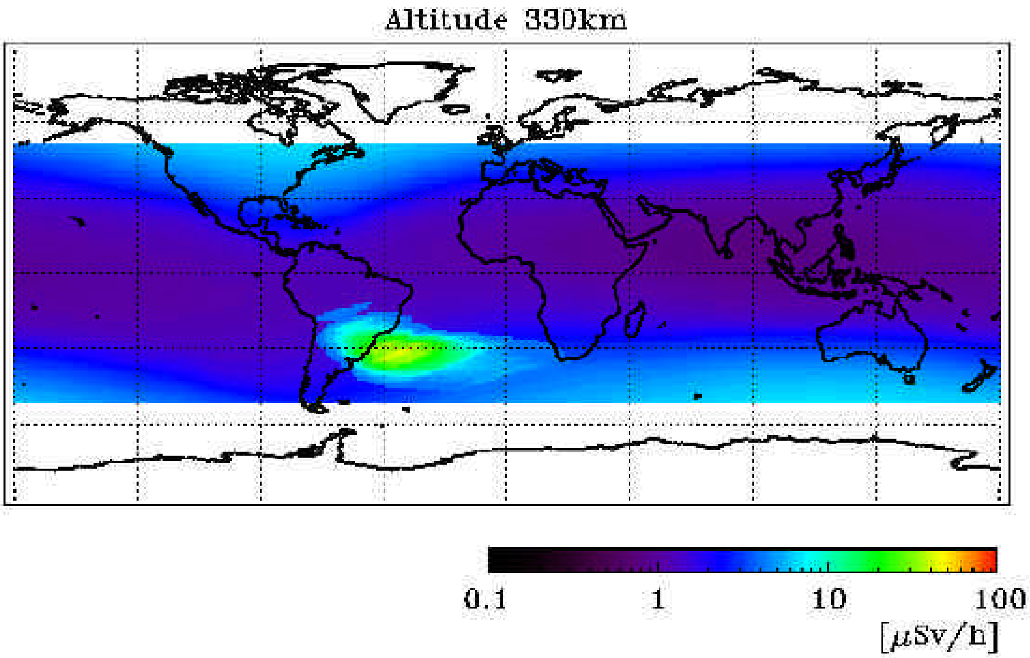

# 8. Altitude Dependence of Dose-Equivalent Rate

Geomagnetic cut-off rigidity and trapped-proton integrated flux are calculated from altitude of 300km through 500km in each 10km step. Each dose-equivalent rate distribution is estimated separately, and summed at final.

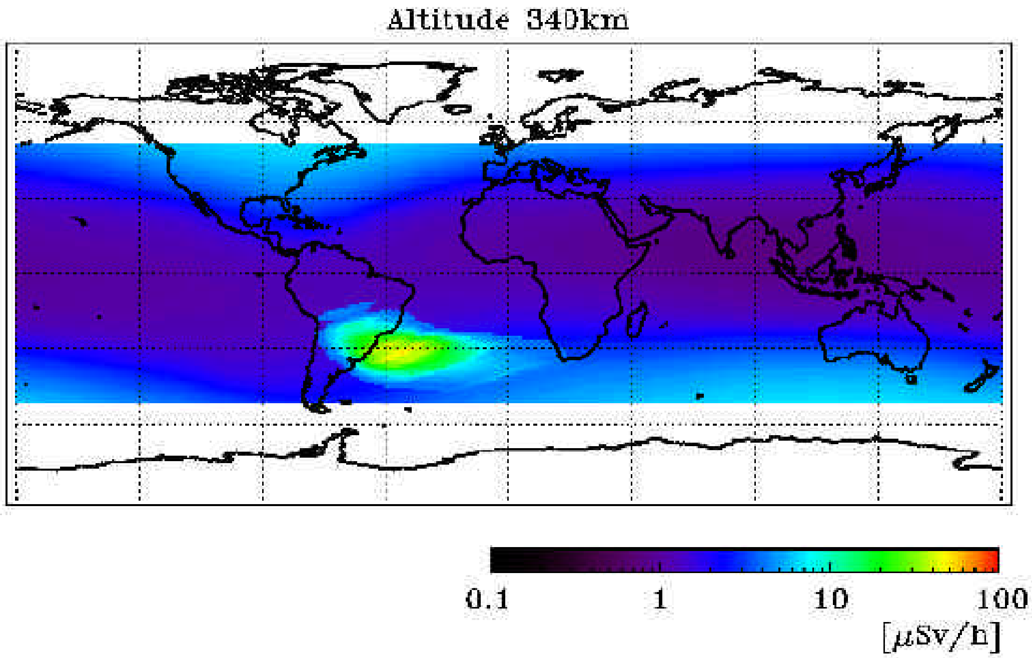

# 8. Altitude Dependence of Dose-Equivalent Rate

Geomagnetic cut-off rigidity and trapped-proton integrated flux are calculated from altitude of 300km through 500km in each 10km step. Each dose-equivalent rate distribution is estimated separately, and summed at final.

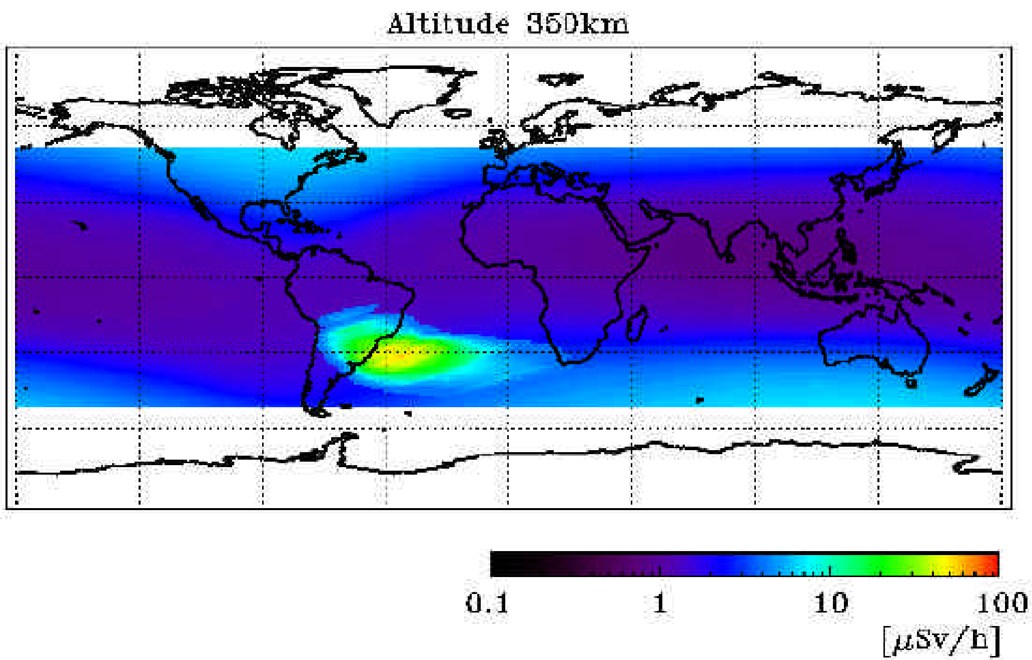

# 8. Altitude Dependence of Dose-Equivalent Rate

Geomagnetic cut-off rigidity and trapped-proton integrated flux are calculated from altitude of 300km through 500km in each 10km step. Each dose-equivalent rate distribution is estimated separately, and summed at final.

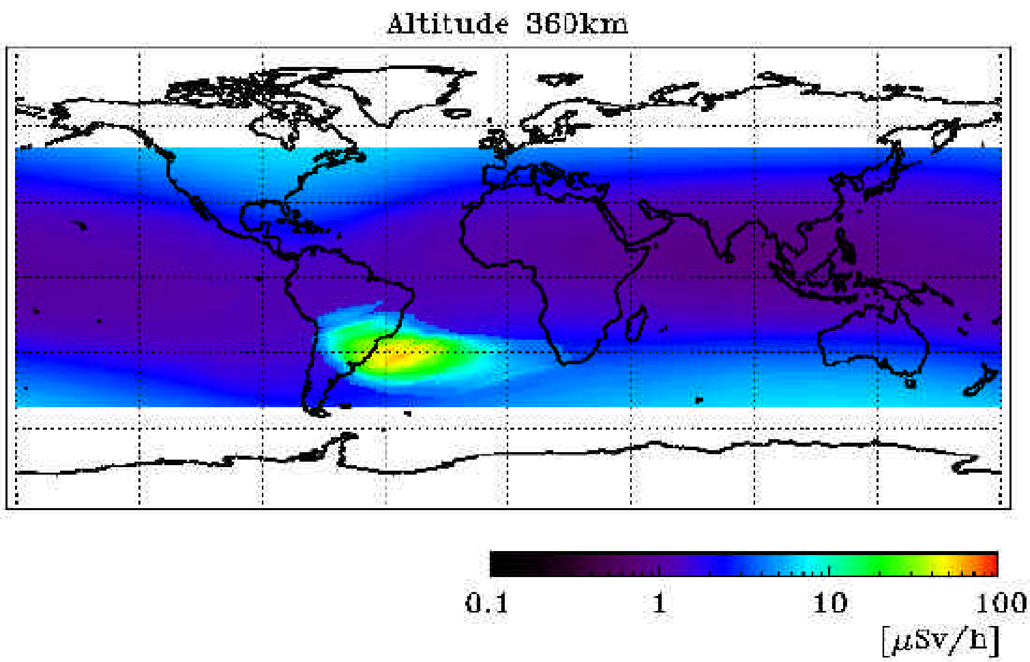

# 8. Altitude Dependence of Dose-Equivalent Rate

Geomagnetic cut-off rigidity and trapped-proton integrated flux are calculated from altitude of 300km through 500km in each 10km step. Each dose-equivalent rate distribution is estimated separately, and summed at final.

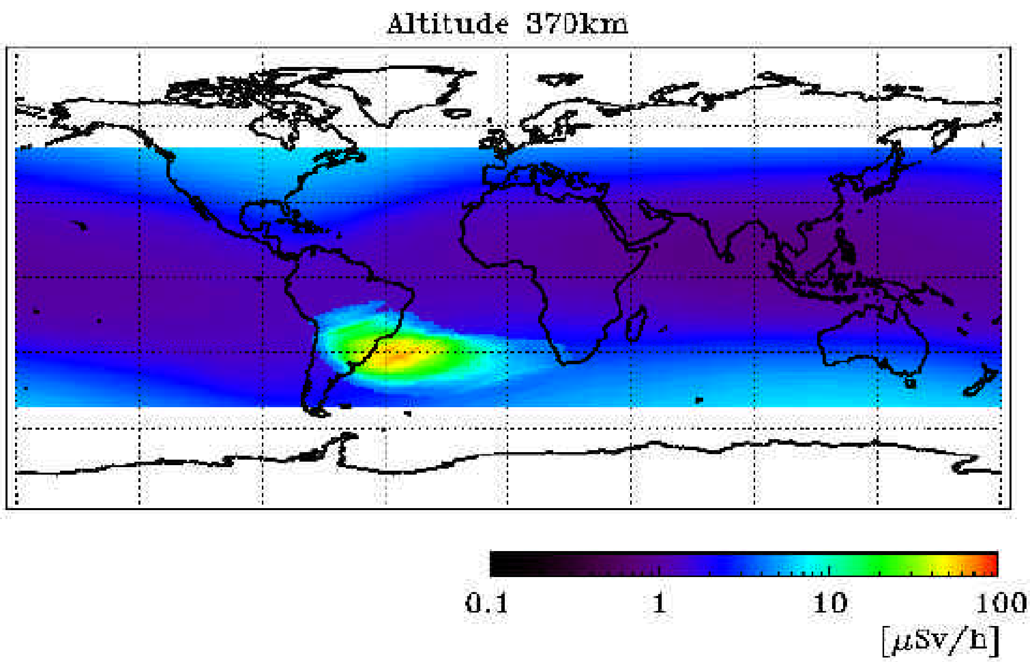

# 8. Altitude Dependence of Dose-Equivalent Rate

Geomagnetic cut-off rigidity and trapped-proton integrated flux are calculated from altitude of 300km through 500km in each 10km step. Each dose-equivalent rate distribution is estimated separately, and summed at final.

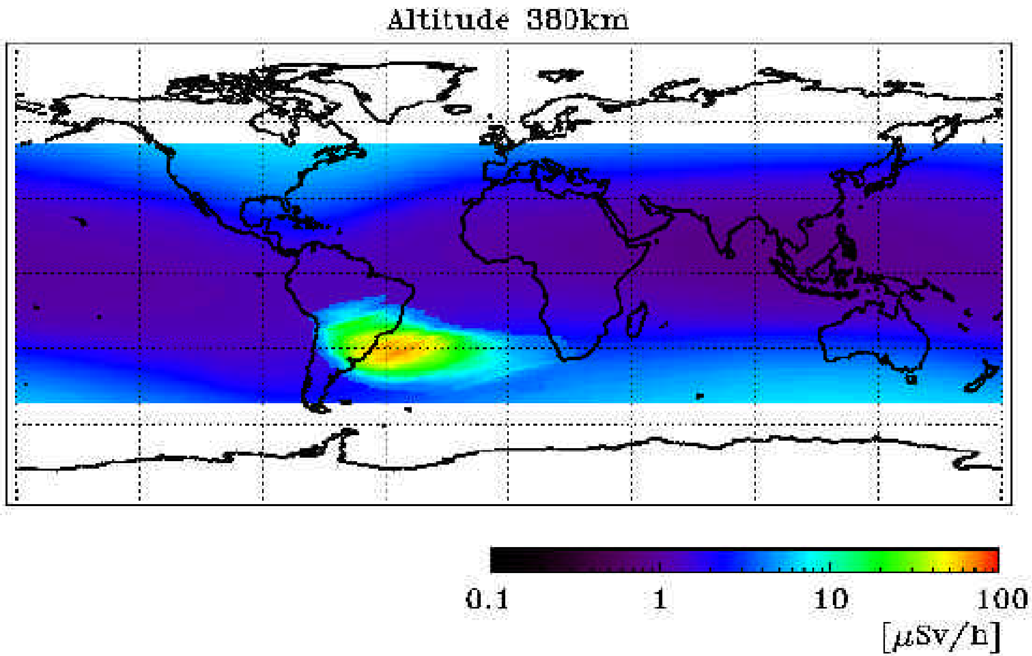

# 8. Altitude Dependence of Dose-Equivalent Rate

Geomagnetic cut-off rigidity and trapped-proton integrated flux are calculated from altitude of 300km through 500km in each 10km step. Each dose-equivalent rate distribution is estimated separately, and summed at final.

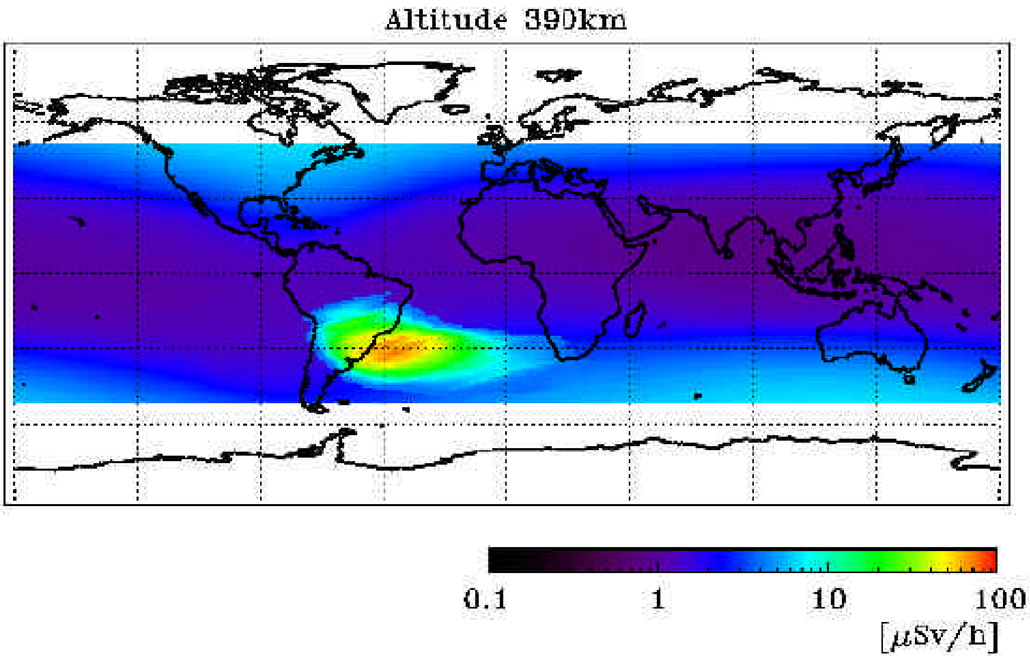

# 8. Altitude Dependence of Dose-Equivalent Rate

Geomagnetic cut-off rigidity and trapped-proton integrated flux are calculated from altitude of 300km through 500km in each 10km step. Each dose-equivalent rate distribution is estimated separately, and summed at final.

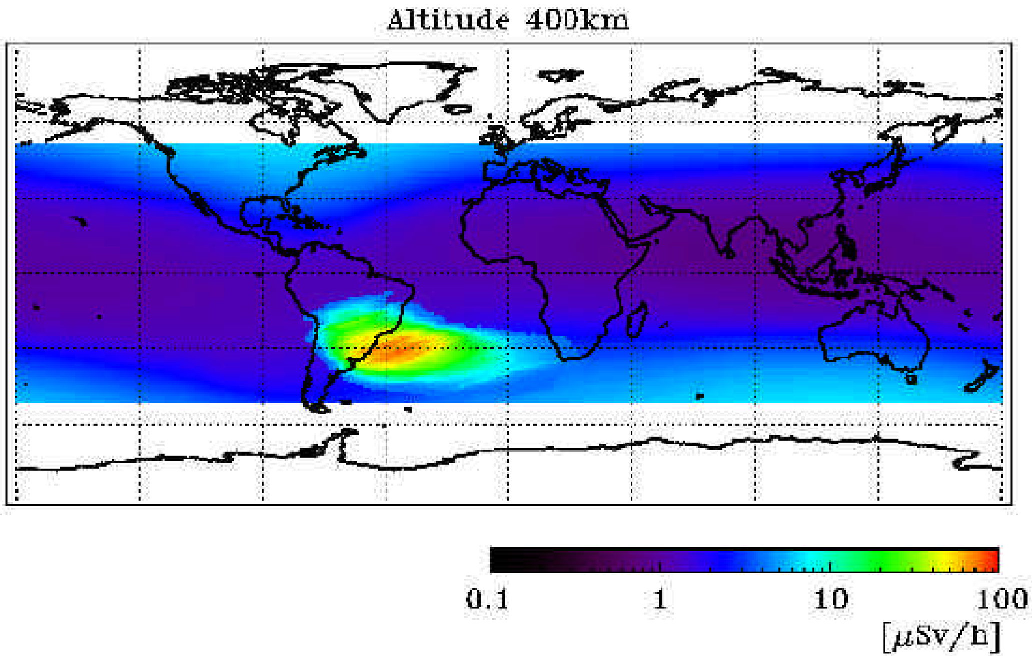

# 8. Altitude Dependence of Dose-Equivalent Rate

Geomagnetic cut-off rigidity and trapped-proton integrated flux are calculated from altitude of 300km through 500km in each 10km step. Each dose-equivalent rate distribution is estimated separately, and summed at final.

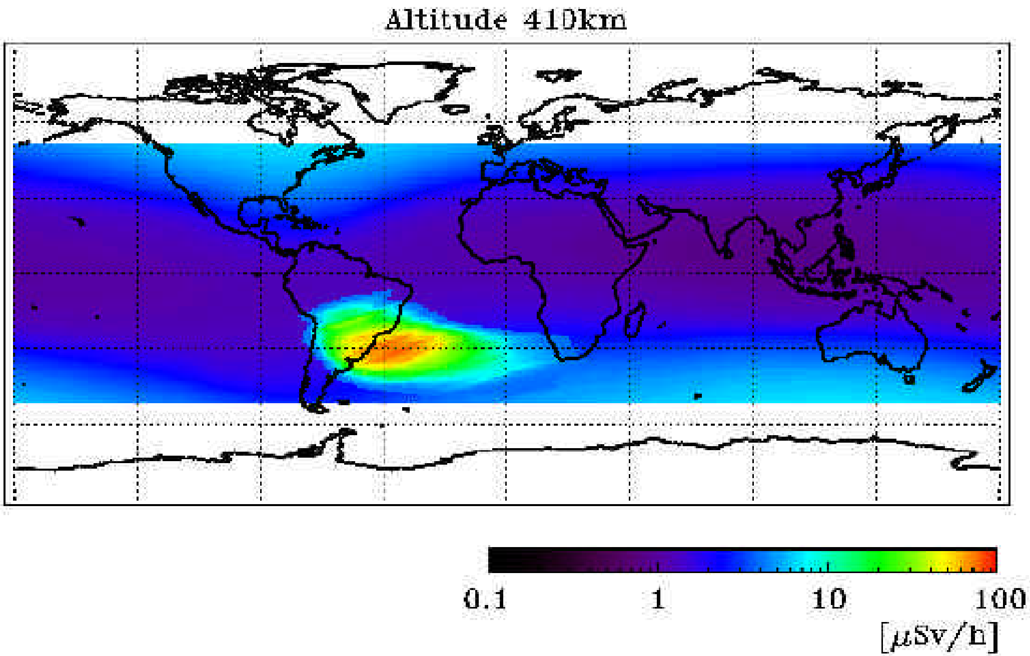

# 8. Altitude Dependence of Dose-Equivalent Rate

Geomagnetic cut-off rigidity and trapped-proton integrated flux are calculated from altitude of 300km through 500km in each 10km step. Each dose-equivalent rate distribution is estimated separately, and summed at final.

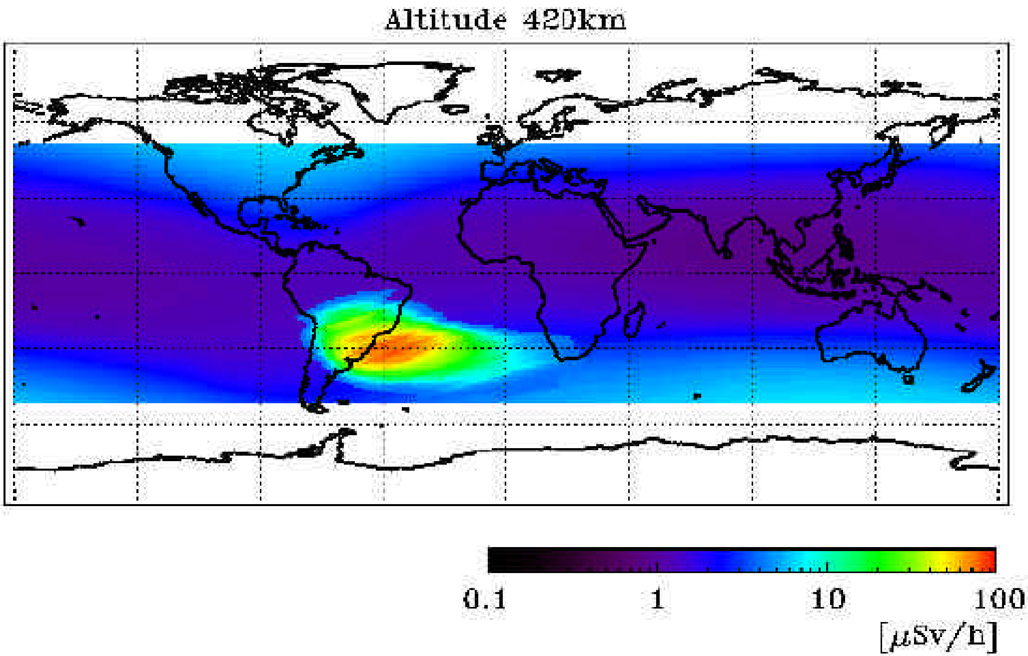

# 8. Altitude Dependence of Dose-Equivalent Rate

Geomagnetic cut-off rigidity and trapped-proton integrated flux are calculated from altitude of 300km through 500km in each 10km step. Each dose-equivalent rate distribution is estimated separately, and summed at final.

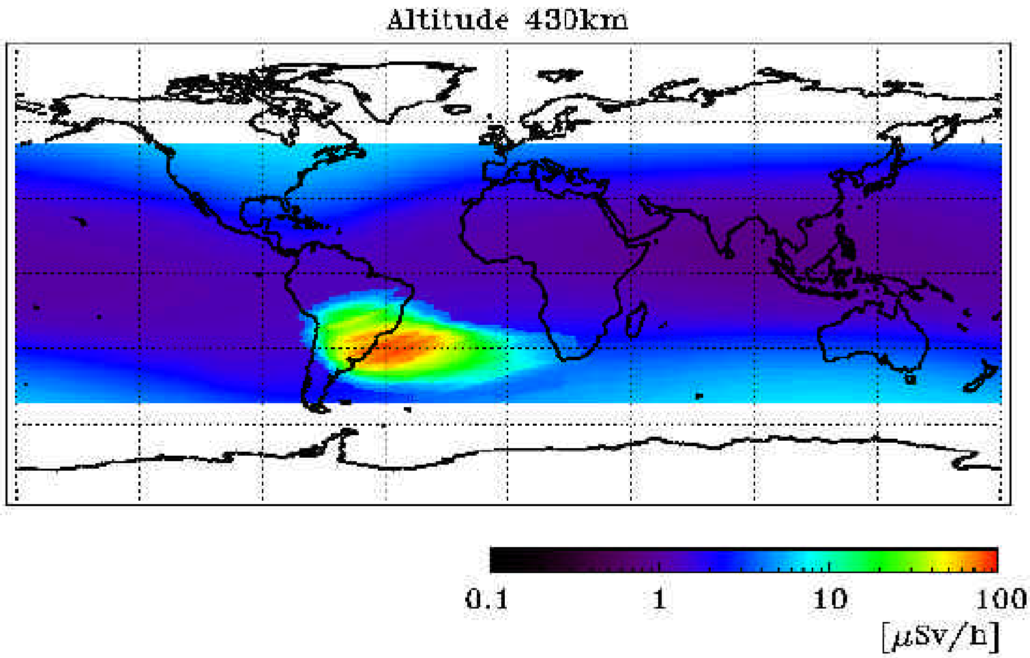

# 8. Altitude Dependence of Dose-Equivalent Rate

Geomagnetic cut-off rigidity and trapped-proton integrated flux are calculated from altitude of 300km through 500km in each 10km step. Each dose-equivalent rate distribution is estimated separately, and summed at final.

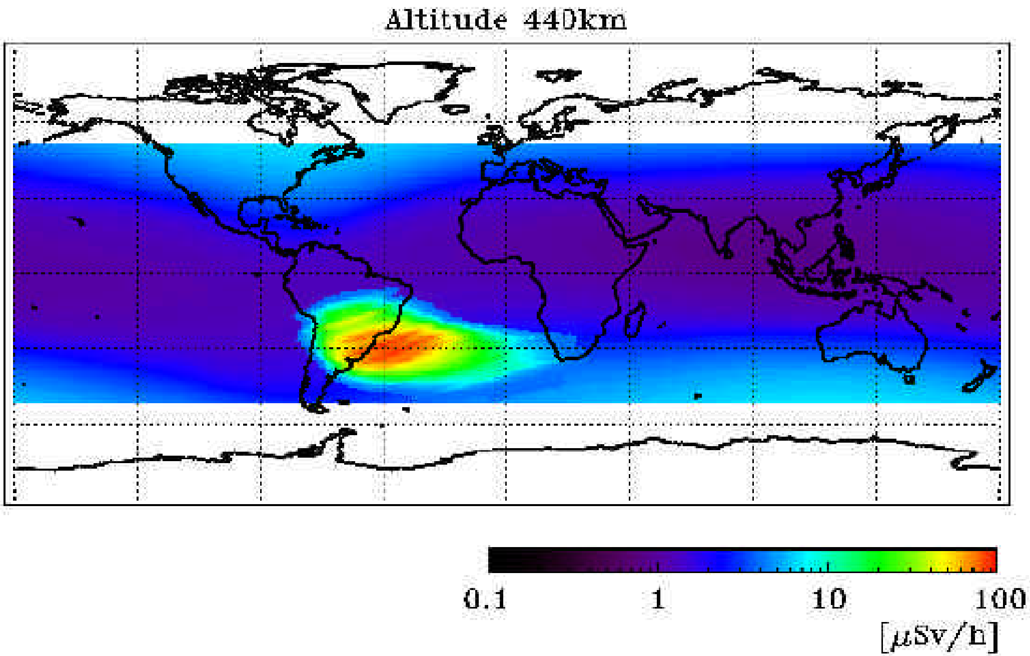

# 8. Altitude Dependence of Dose-Equivalent Rate

Geomagnetic cut-off rigidity and trapped-proton integrated flux are calculated from altitude of 300km through 500km in each 10km step. Each dose-equivalent rate distribution is estimated separately, and summed at final.

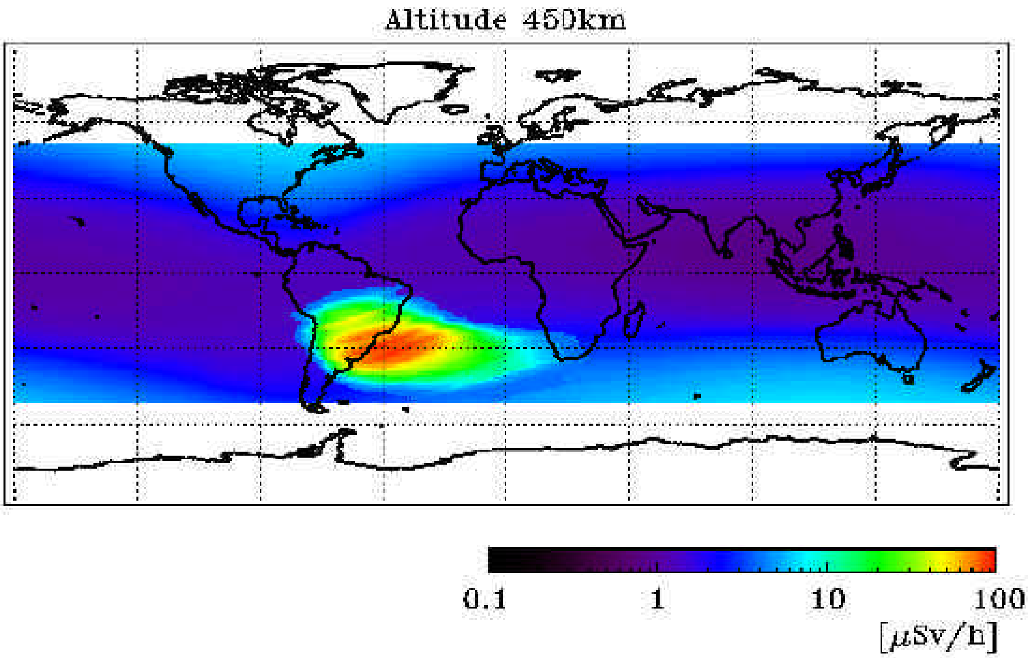

# 8. Altitude Dependence of Dose-Equivalent Rate

Geomagnetic cut-off rigidity and trapped-proton integrated flux are calculated from altitude of 300km through 500km in each 10km step. Each dose-equivalent rate distribution is estimated separately, and summed at final.

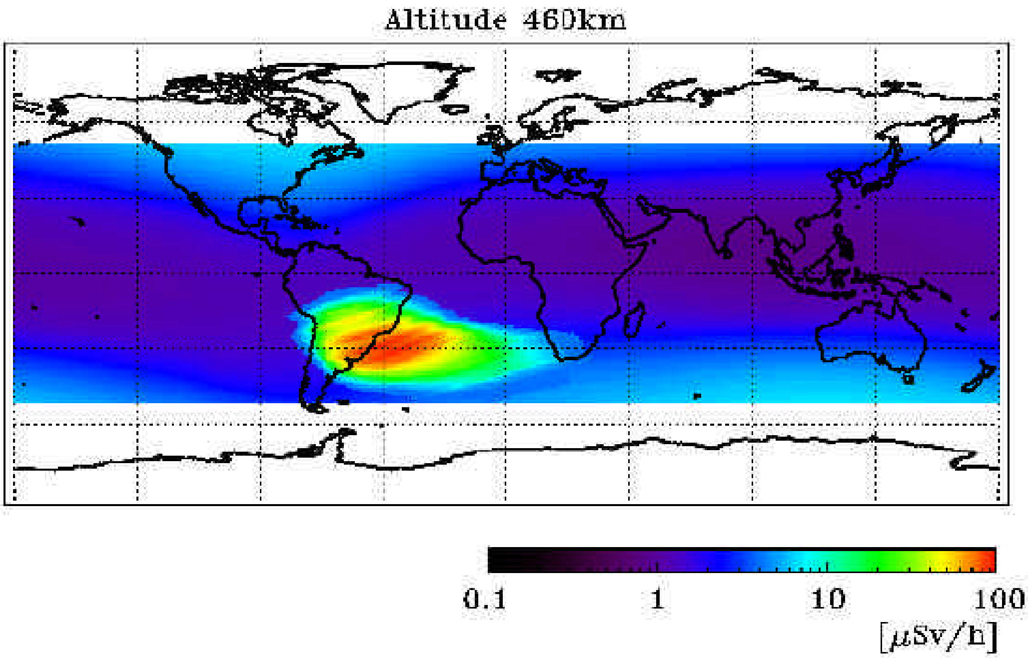

# 8. Altitude Dependence of Dose-Equivalent Rate

Geomagnetic cut-off rigidity and trapped-proton integrated flux are calculated from altitude of 300km through 500km in each 10km step. Each dose-equivalent rate distribution is estimated separately, and summed at final.

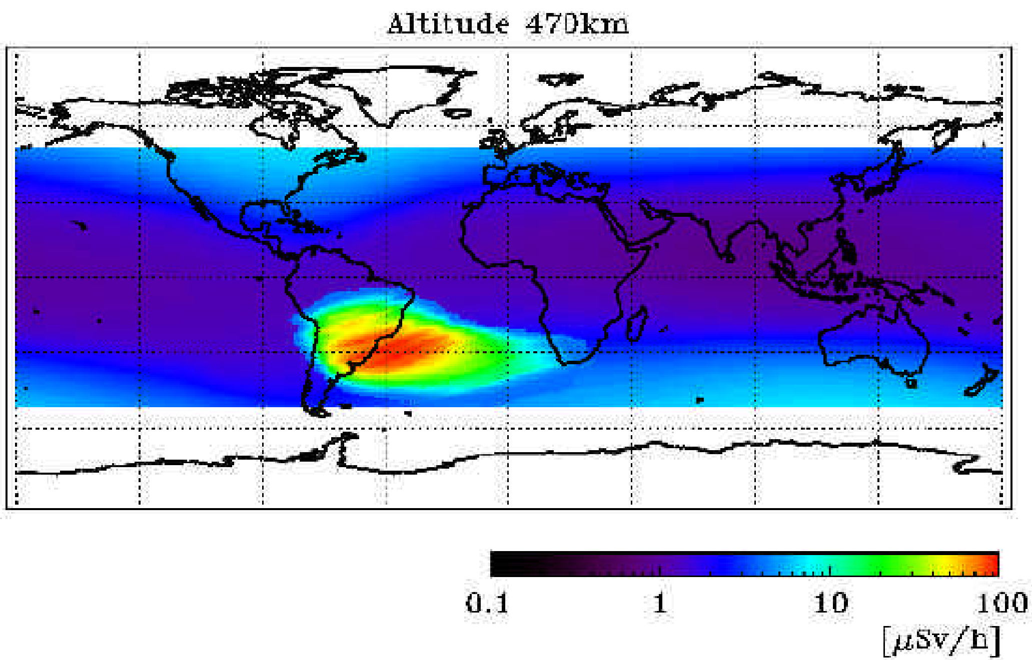

# 8. Altitude Dependence of Dose-Equivalent Rate

Geomagnetic cut-off rigidity and trapped-proton integrated flux are calculated from altitude of 300km through 500km in each 10km step. Each dose-equivalent rate distribution is estimated separately, and summed at final.

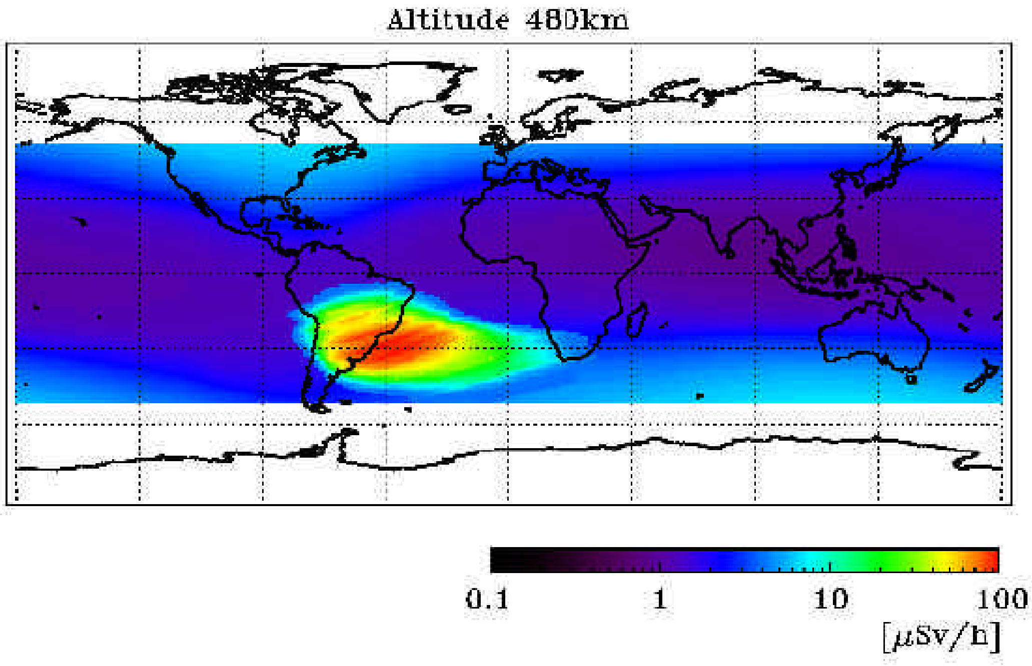

# 8. Altitude Dependence of Dose-Equivalent Rate

Geomagnetic cut-off rigidity and trapped-proton integrated flux are calculated from altitude of 300km through 500km in each 10km step. Each dose-equivalent rate distribution is estimated separately, and summed at final.

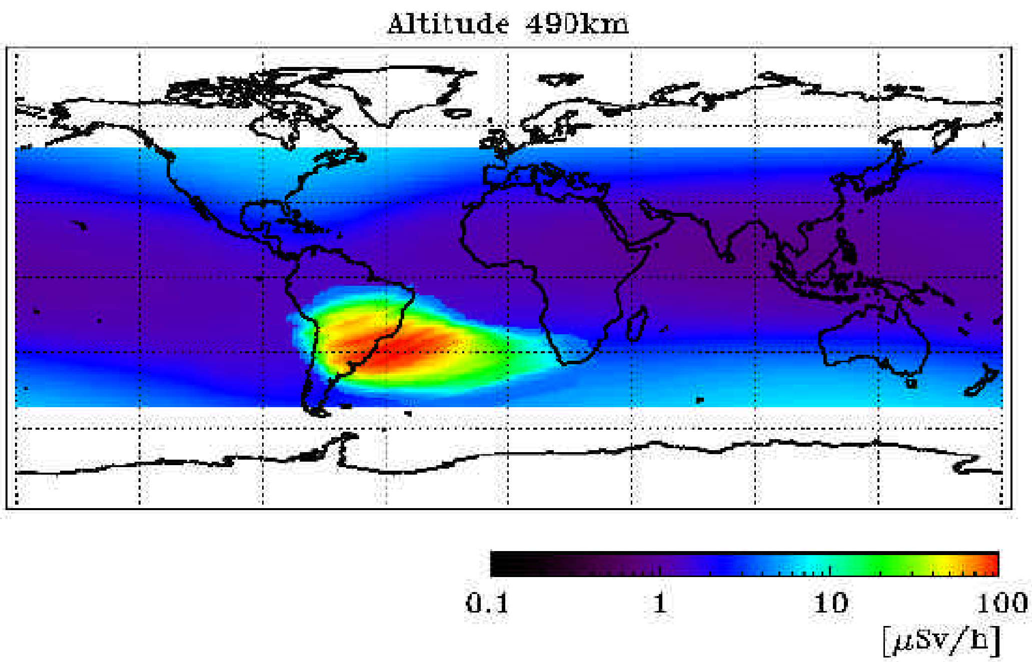

# 8. Altitude Dependence of Dose-Equivalent Rate

Geomagnetic cut-off rigidity and trapped-proton integrated flux are calculated from altitude of 300km through 500km in each 10km step. Each dose-equivalent rate distribution is estimated separately, and summed at final.

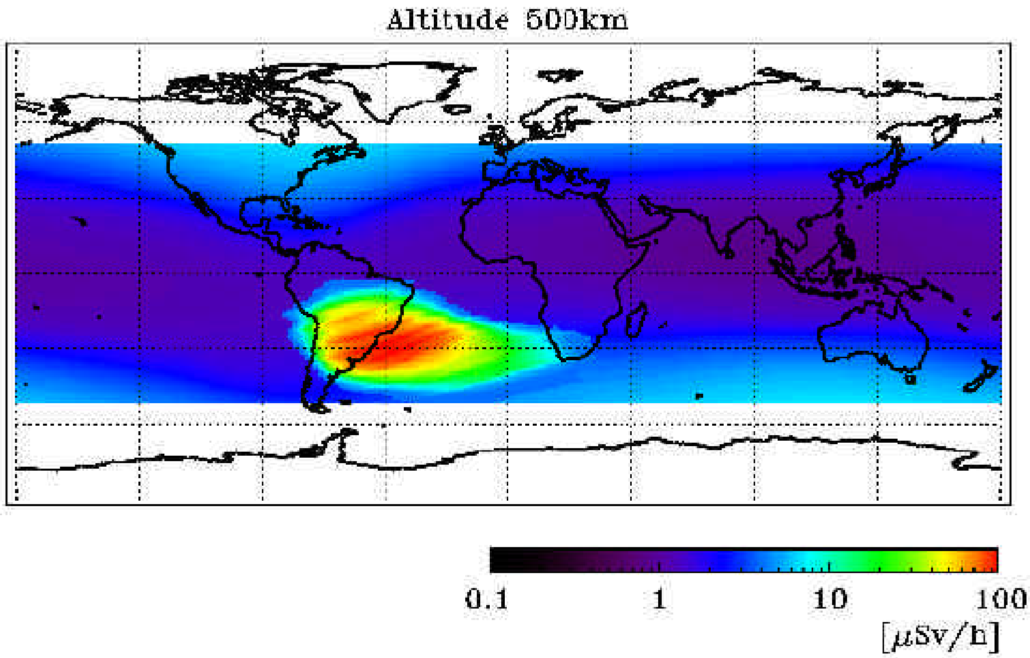

# 8. Altitude Dependence of Dose-Equivalent Rate

Dose-equivalent rate increases two times from 300km to 500km, which is smaller than that for charged particles, because…

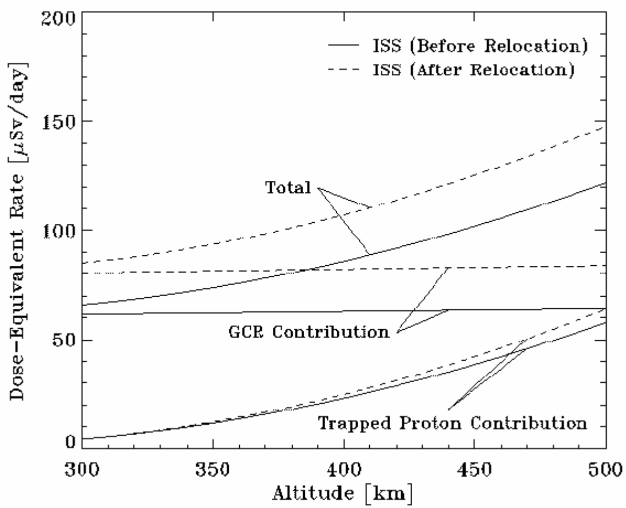

# 8. Altitude Dependence of Dose-Equivalent Rate

Dose-equivalent rate increases two times from 300km to 500km, which is smaller than that for charged particles, because…

Trapped-proton contribution rapidly increases.

GCR contribution is almost same.

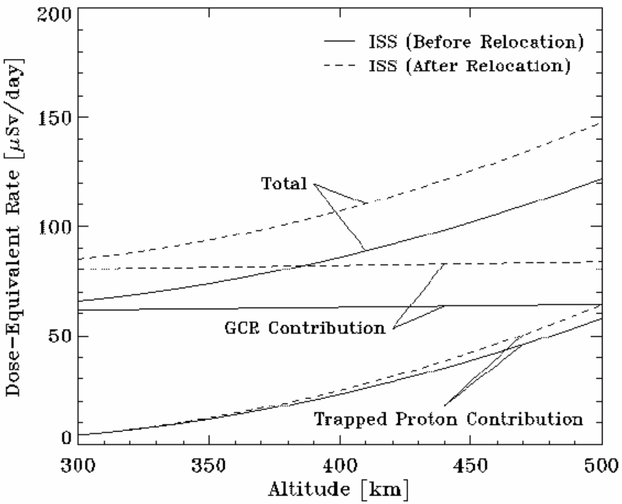

# 8. Altitude Dependence of Dose-Equivalent Rate

Dose-equivalent rate increases two times from 300km to 500km, which is smaller than that for charged particles, because...

Trapped-proton contribution rapidly increases

GCR contribution is almost same

The ratio of GCR contribution to trapped-proton contribution through the BBND experiment is about 3, which is higher than that for charged particles.

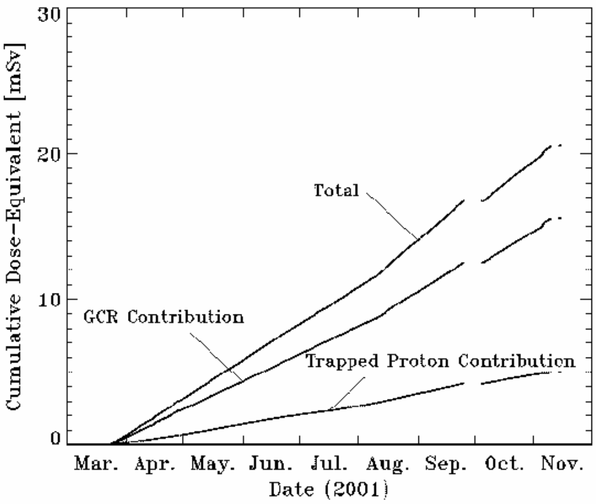

# 8. Altitude Dependence of Dose-Equivalent Rate

Dose-equivalent rate increases two times from 300km to 500km, which is smaller than that for charged particles, because...

Trapped-proton contribution rapidly increases

GCR contribution is almost same

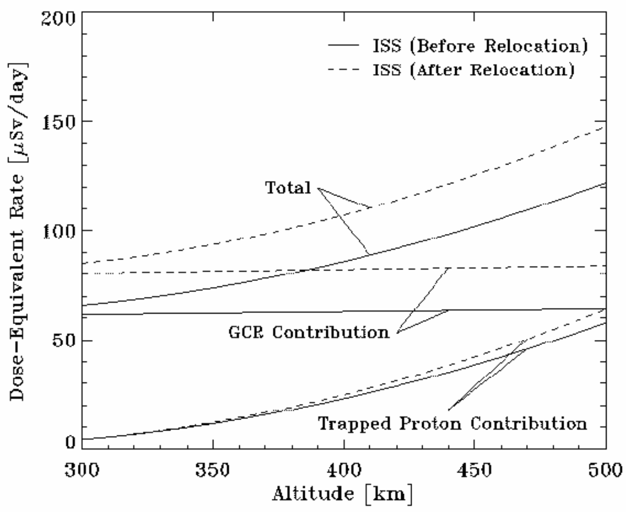


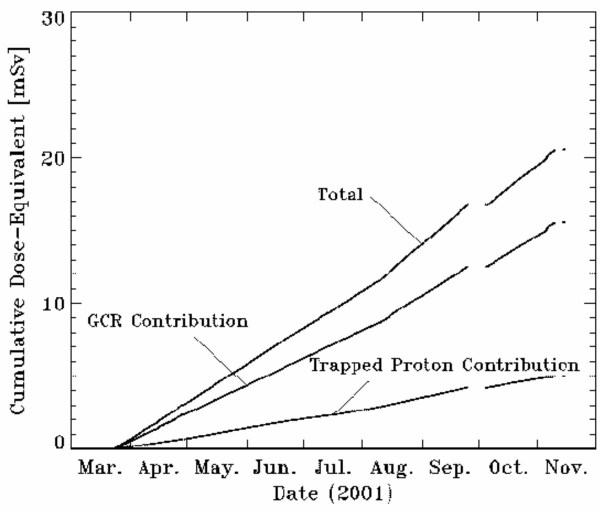

# 9. Influences of Solar Phenomena

An energetic flare and coronal mass ejection (CME) occurred on 4th Nov. 2001, which caused largest influences on the radiation environment on the ISS orbit during the BBND experiment.

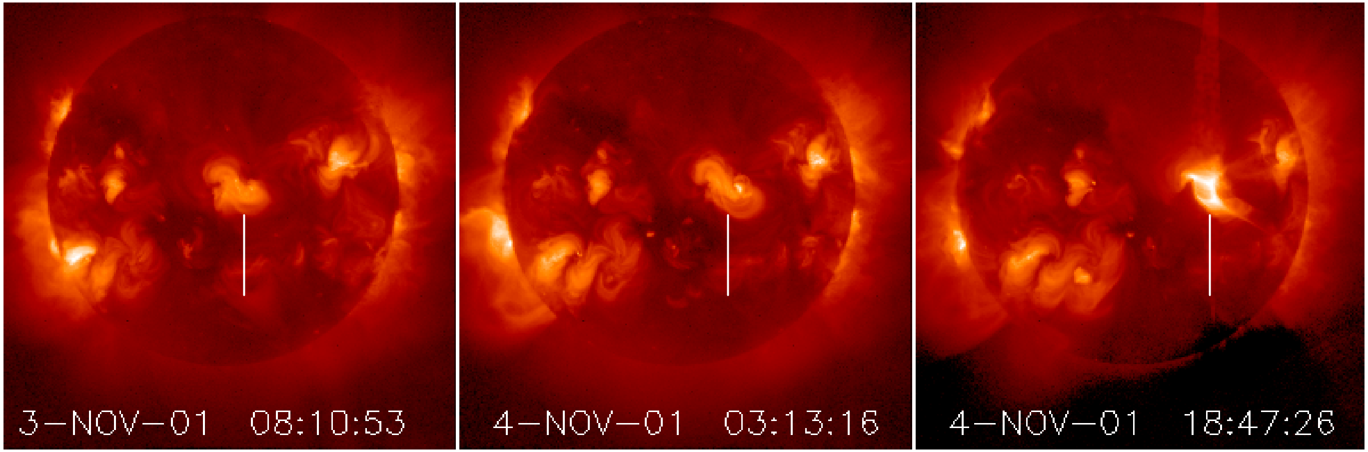

# 9. Influences of Solar Phenomena

An energetic flare and coronal mass ejection (CME) occurred on 4th Nov. 2001, which caused largest influences on the radiation environment on the ISS orbit during the BBND experiment.

The solar x-ray flux and the energetic proton flux observed by the GOES satellite at geo-stationary earth orbit show that about a few hours after the solar event occurrence, the large geomagnetic storm begun and continued for a few days.

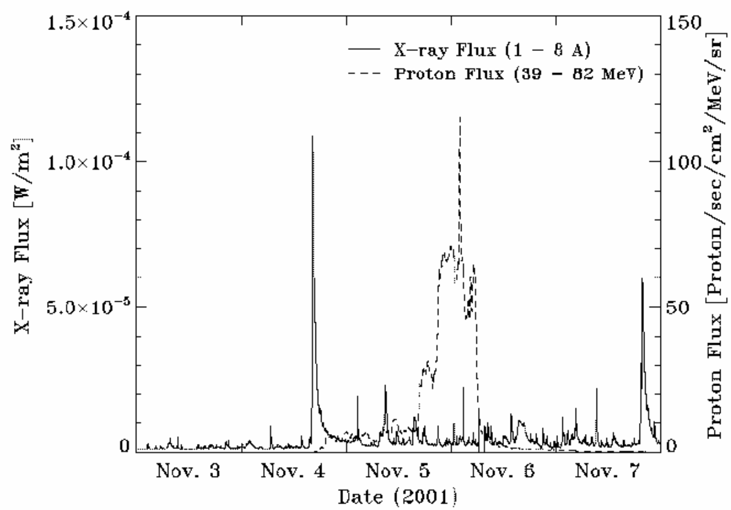

# 9. Influences of Solar Phenomena

Influences of solar phenomena appears in high-latitude region.

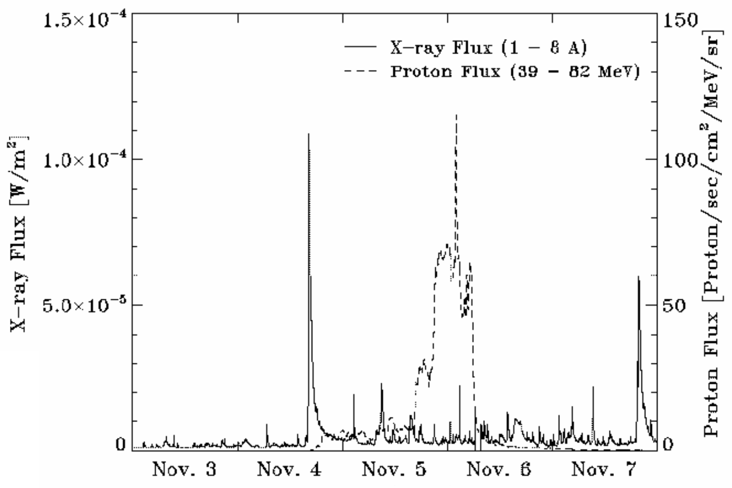


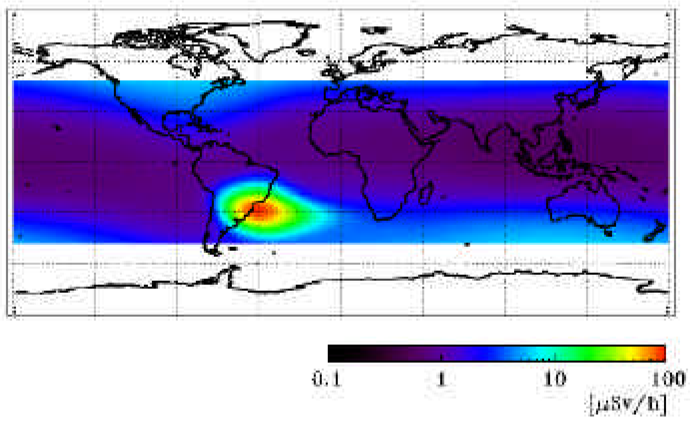


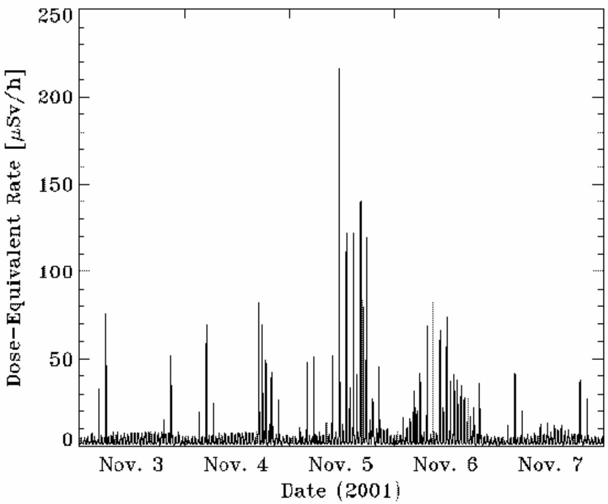

# 9. Influences of Solar Phenomena

Influences of solar phenomena appears in high-latitude region.

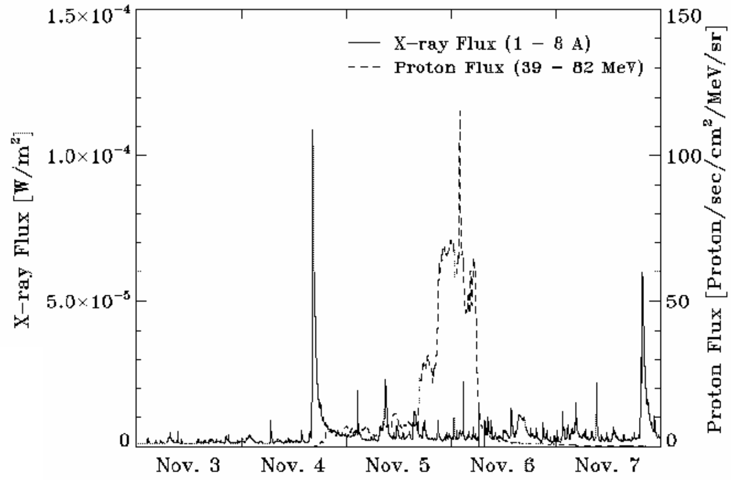


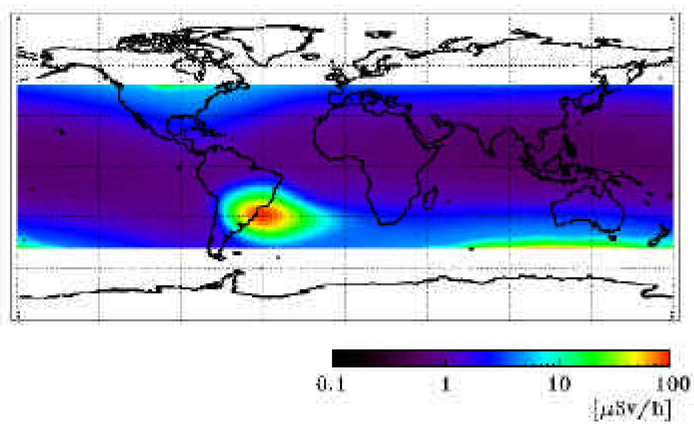


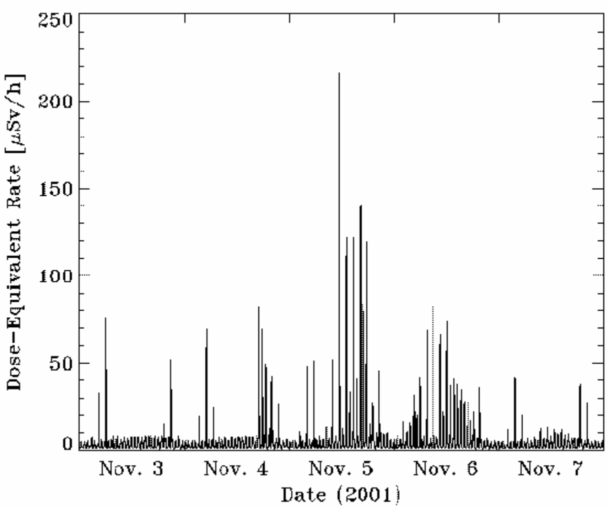

# 9. Influences of Solar Phenomena

The whole influences of this solar phenomena is evaluated to be 0.19mSv.

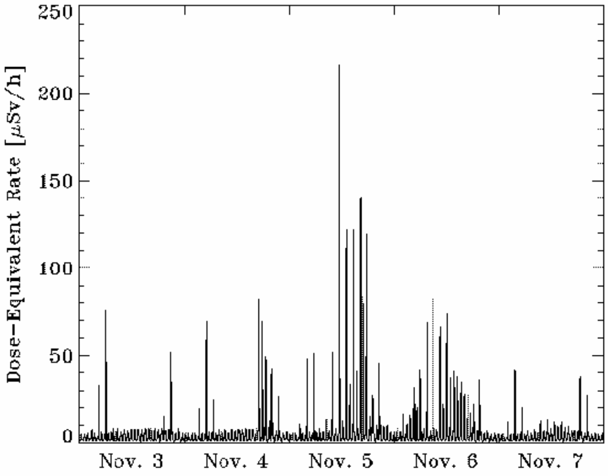


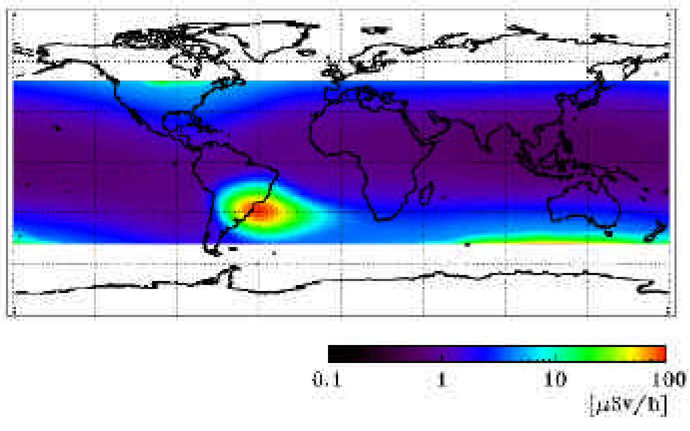


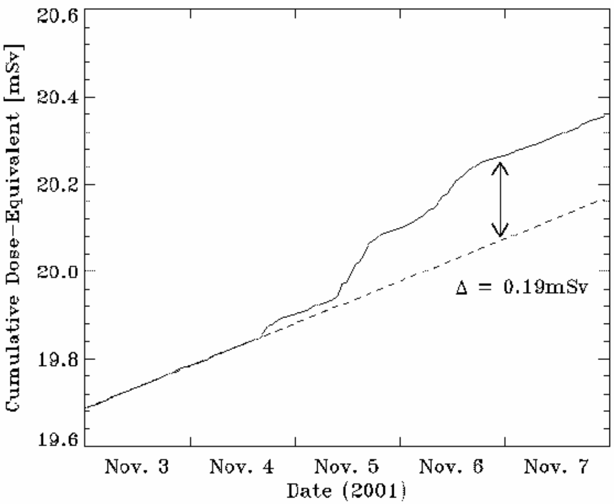

# 9. Influences of Solar Phenomena

The whole influences of this solar phenomena is evaluated to be 0.19mSv.

This was less than 1% of annual dose-equivalent of 34mSv estimated by the average dose-equivalent rate.

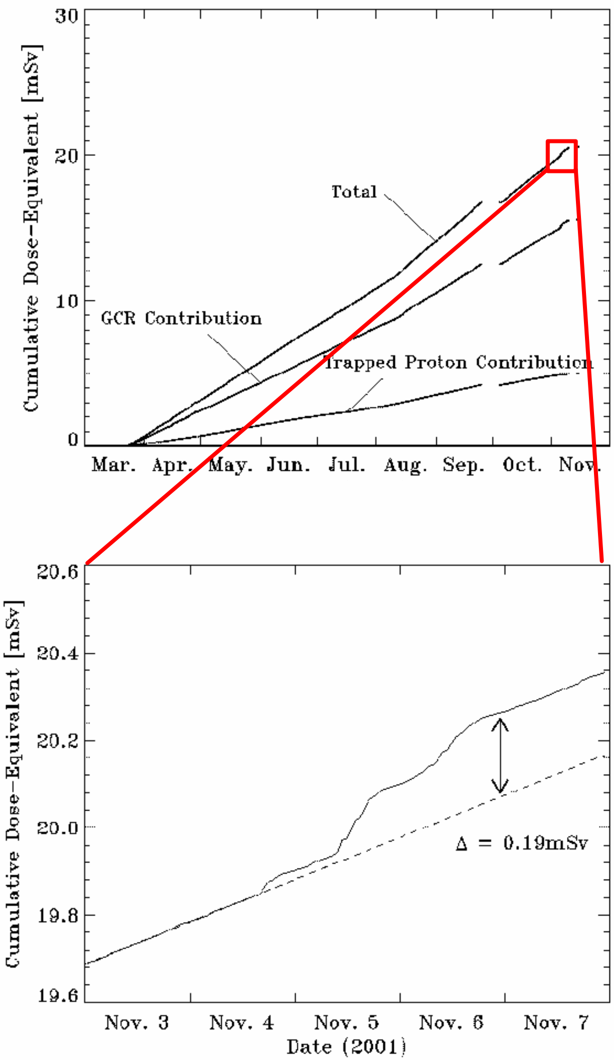

# 10. Conclusion

The BBND experiment was successfully conducted for about 8 months in 2001 on the US Laboratory Module of the ISS. Based on the obtained data, the neutron radiation environment inside the ISS can be evaluated.

# 10. Conclusion

The BBND experiment was successfully conducted for about 8 months in 2001 on the US Laboratory Module of the ISS. Based on the obtained data, the neutron radiation environment inside the ISS can be evaluated.

The average dose-equivalent rate 85μSv/d (before relocation) and 109μSv/d (after relocation). By using two relations of geomagnetic cut-off rigidity and trapped-proton integrated flux with dose-equivalent rate, its altitude dependence from 300km through 500km is briefly estimated.

# 10. Conclusion

The BBND experiment was successfully conducted for about 8 months in 2001 on the US Laboratory Module of the ISS. Based on the obtained data, the neutron radiation environment inside the ISS can be evaluated.

The average dose-equivalent rate 85μSv/d (before relocation) and 109μSv/d (after relocation). By using two relations of geomagnetic cut-off rigidity and trapped-proton integrated flux with dose-equivalent rate, its altitude dependence from 300km through 500km is briefly estimated.

The most influenced solar phenomenon during the BBND experiment was the solar flare associated with the CME occurred on 4$^{th}$ Nov. 2001, the whole influence of which was 0.19mSv, less than 1% of annual dose-equivalent.